Vertical Velocities and Transports in the Equatorial Pacific during 1993–99*

CHRISTOPHER S. MEINEN+

Joint Institute for the Study of the Atmosphere and Ocean, University of Washington, Seattle, Washington

MICHAEL J. MCPHADEN AND GREGORY C. JOHNSON

NOAA/Pacific Marine Environmental Laboratory, Seattle, Washington

(Manuscript received 31 August 2000, in final form 30 March 2001)

ABSTRACT

Geostrophic and Ekman transports calculated from observations of subsurface thermal structure and surface winds are used to determine vertical velocities and transports as a function of time, depth, and longitude in the equatorial Pacific within 5°S–5°N, 165°E–95°W during 1993–99 via a box volume balance. The vertical transports are determined in boxes of 10° of latitude by generally 15° in longitude. The corresponding vertical velocities represent a spatial average over these regions. Both the total vertical velocity and the cross-isopycnal component of the vertical velocity (approximated by the cross-isothermal component) are calculated on seasonal and interannual timescales. For the eastern equatorial Pacific (5°S–5°N, 155°–95°W) the mean vertical transport across 50 m is $(24 \pm 3) \times 10^6$ m^3 s^{-1}. Variability in the vertical velocity is large relative to the mean. On interannual timescales this variability is well correlated with the local winds in the western portion of the study area, while the correspondence is weaker in the east where wind variability is much smaller. At seasonal timescales there is good correspondence between the vertical velocity and the local winds throughout the study region. The cross-isothermal vertical velocity is significantly smaller than the total vertical velocity, and the means of both compare well with the few historical estimates available.

1. Introduction

Vertical water movement in the equatorial Pacific ocean changes sea surface temperatures (SST), provides nutrients for biological organisms in the near-surface waters, and forms one part of the subtropical meridional overturning cells that extend poleward from the equatorial region. Both the total vertical velocity (w) and the cross-isothermal component of the vertical velocity (w_{ci}) are of importance, for different reasons. Near the equator, for example, w advects nutrients up into the euphotic zone where they can be used by biological organisms, while w_{ci} plays an important role in the heat budget because it represents that part of the vertical velocity field involving diabatic processes and water mass conversions (Bennet 1986; Brady and Bryden 1987).

The existence of significant w on the equator has been recognized for several decades (Cromwell 1953; Knauss 1963; Wyrtki 1981; Wyrtki and Eldin 1982). The determination of the magnitude of w, however, is quite challenging. At the timescales of interest here (i.e., longer than a month) w is orders of magnitude smaller than the horizontal water velocities and is very difficult to measure directly. Most studies have instead tried to obtain estimates of w indirectly from one of several methods: by diagnosing it from a small number of moorings in cross-shaped or triangle-shaped deployments using horizontal divergence in combination with the continuity equation (Halpern and Freitag 1987; Halpern et al. 1989; Qiao and Weisberg 1997; Weisberg and Qiao 2000); by applying the continuity equation to horizontal divergence estimated from shipboard acoustic Doppler current profiler (ADCP) sections (Johnson and Luther 1994; Johnson et al. 2001); by applying geostrophic and Ekman dynamics to historical hydrography and wind data in a box volume balance (Wyrtki 1981; Bryden and Brady 1985; Meinen and McPhaden 2001); by directly measuring the mixed layer divergence using surface drifters (Hansen and Paul 1987; Poulain 1993); or by inferring w from tracer measurements (Quay et al. 1983; Fine et al. 1983). Because of data limitations most of these studies have been restricted to determining w at either a single point within, or over limited areas of, the

* Pacific Marine Environmental Laboratory Contribution Number 2236, and Joint Institute for the Study of the Atmosphere and Ocean Contribution Number 786.

+ Current affiliation: Department of Oceanography, University of Hawaii at Manoa, Honolulu, Hawaii.

Corresponding author address: Dr. Christopher S. Meinen, Department of Oceanography, University of Hawaii at Manoa, 1000 Pope Road, MSB 205, Honolulu, HI 96822.
E-mail: cmeinen@soest.hawaii.edu

equatorial region. None of these historical efforts had data over a long enough period to do a detailed study of the seasonal and interannual variability of w in the equatorial Pacific (for the purposes of this paper interannual variability refers to all timescales within our time series that are longer than seasonal). Modeling studies have been used to look at the variability of w but there was little or no data against which to validate the model outputs (Philander et al. 1987; Harrison 1996; Kessler et al. 1998).

A recent study documented the horizontal transports (geostrophic and Ekman) in the equatorial Pacific using subsurface temperature data from moorings and shipboard measurements in concert with wind datasets (Meinen and McPhaden 2001). Significant meridional and zonal transport variability occurs on interannual timescales during 1993–99 as warm water is exchanged between the higher latitudes and the equatorial region. That study also quantified w_{ci} across the 20°C isotherm during 1993–99, a period that included weak interannual variations during 1993–96 and major climatic swings associated with the 1997–98 El Niño and 1998–99 La Niña events (McPhaden 1999). The cross-isotherm vertical velocity was calculated over two regions: within 8°S–8°N, 156°E–155°W; and within 8°S–8°N, 155°–95°W. Peak-to-peak vertical cross-isotherm transport (W_{ci}) changes of as much as 50 Sv (Sv $\equiv 10^6$ m^3 s^{-1}) were observed between the 1997–98 El Niño and 1998–99 La Niña events.

The purpose of this study is to estimate the mean w and its variability on seasonal and interannual timescales in the equatorial region during the 1993–99 time period. A box volume balance is applied using essentially the same horizontal velocities as in Meinen and McPhaden (2001). However, here we examine the vertical velocity variability with higher vertical and zonal resolution within the region 5°S–5°N, 165°E–95°W. The paper is organized as follows. The observations used for the study are described in section 2. The method of estimating the horizontal divergence, w, and w_{ci} is discussed in section 3. The results are shown and discussed in section 4. A summary is presented in section 5. A discussion of the estimated errors appears in the appendix.

2. Data

Gridded surface and subsurface temperature measurements were provided by Neville Smith of the Bureau of Meterology Research Centre (BMRC), Australia (Smith 1995a,b). The BMRC dataset combines XBT data with data from moorings, where available, using an optimal interpolation process to create a gridded dataset with monthly values at every 1° of latitude and every 2° of longitude at a set of 14 depths between the surface and 500 m. Since about 1993, roughly three quarters of the subsurface temperature information in the BMRC data analysis between 5°S and 5°N derives from the Tropical Atmosphere and Ocean (TAO) Array (Smith and Meyers 1996). The TAO array consists of almost 70 ATLAS (Autonomous Temperature Line Acquisition System) moorings spanning the equatorial Pacific from 8°S to 8°N, 137°E to 95°W (McPhaden et al. 1998). The ATLAS moorings measure subsurface temperature at 10 depths in the upper 500 m as well as sea surface temperature (SST), wind speed and direction, and other surface meteorological parameters. A few current meter moorings are deployed along the equator. The limited spatial coverage of the velocity data, however, reduces their usefulness for the purposes of this study.

The Reynolds SST analysis, which represents a blending of satellite-based and in situ SST measurements (Reynolds 1988; Reynolds and Smith 1995), was also used for this study. These SST data are available on a 1° by 1° grid at weekly time intervals. We calculated monthly averages for comparison with the other datasets.

Three different wind products were used for calculating Ekman transports as part of this study. The FSU wind dataset, which combines measurements from ships and buoys, provides monthly wind pseudostress on a 2° by 2° grid. These data are provided by J. J. O'Brien and D. M. Legler at The Florida State University via their Web site (http://www.coaps.fsu.edu/woce/). A second wind dataset was obtained from the European Centre for Medium-Range Weather Forecasts. The ECMWF winds are on a 2.5° by 2.5° grid and are derived from an atmospheric general circulation model, which assimilates measurements from many data sources including ship and TAO buoy winds. We processed twice daily ECMWF analyses to monthly means for this study. A third wind dataset was obtained from the scatterometer measurements from the *ERS-1*, *ERS-2*, and National Aeronautics and Space Administration Scatterometer satellites (henceforth referred to as SCAT). The SCAT measurements were blended into a weekly data set on a 1° by 1° grid distributed by the Institut Français de Recherche pour l'Exploitation de la Mer (IFREMER; http://www.ifremer.fr/cersat/). From these weekly data we produced monthly mean winds. ECMWF and SCAT wind velocities were converted into wind stress (τ_x, τ_y) using a constant drag coefficient of 1.43×10^{-3} and an air density of 1.225 kg m^{-3} (Weisberg and Wang 1997). The FSU pseudostress was converted to stress using a drag coefficient of 1.20×10^{-3} (Sirven et al. 1998) because the larger drag produced stresses that resulted in unusually large Ekman transports in comparison to the other datasets. While the Ekman transports calculated using the different wind products did show some inconsistencies, the effects of these differences on w were small. For this reason only the results determined using the ECMWF product are shown in this paper. ECMWF winds were chosen because Meinen and McPhaden (2001) demonstrated that the ECMWF-derived Ekman transports consistently agreed with at least one of the other two products throughout 1993–99.

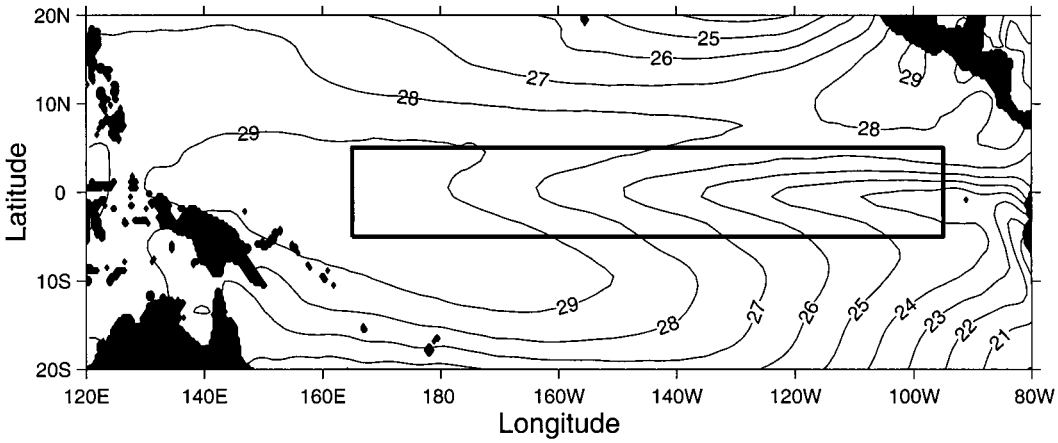

FIG. 1. Location of the study area indicated by box. Shaded areas indicate land. Mean SST is contoured, contour labels are in degrees Celsius.

Throughout the paper all of the datasets have been monthly averaged. Seasonal cycles are determined over the period 1993–96, which included two weak El Niño events in 1993 and 1994/95 as well as a weak La Niña event in 1995/96. The seasonal cycle is defined as the monthly mean over these four years minus the four-year (1993–96) mean. No smoothing is applied to the seasonal cycles. Time series of interannual variability, which have had the seasonal cycle removed, are smoothed with a five-month running mean to remove shorter-scale variability. Some figures include the long-term mean in the interannual variability, some do not, as noted in the figure captions.

3. Methods

The lateral boundaries for our study region (Fig. 1) are chosen as follows. Conventional geostrophic and Ekman dynamics cease to hold for meridional velocities near the equator where the Coriolis parameter f goes to zero. For this reason the meridional boundaries chosen are at 5°S and 5°N where the meridional flows are still well characterized by geostrophic and Ekman dynamics (Lagerloef et al. 1999). The zonal boundaries are chosen to maximize the extent of our region while remaining in the area where sufficient data are available. The western boundary at 165°E is chosen because that was the westernmost line where sufficient shipboard ADCP measurements are available during the 1990s for a 2°S–2°N mean zonal velocity correction (discussed below). Additionally, an examination of the zonal distribution of mean upwelling presented later suggested that the vertical velocities tailed off toward 165°E, consistent with the decrease in the zonal wind stress. The eastern boundary at 95°W is chosen because that was the easternmost line where both TAO array measurements and shipboard ADCP data is available. Furthermore, the meridional divergence in the upper 50 m drops significantly east of 90°W (Poulain 1993).

As mentioned earlier there are insufficient current meter measurements to directly determine horizontal velocity throughout the near-equatorial Pacific. Instead these velocities are inferred from a combination of wind measurements and subsurface temperature measurements. The former provide estimates of the horizontal Ekman transports via the traditional technique of relating surface stress to ocean transports (e.g., Pond and Pickard 1983). The subsurface temperature measurements are combined with historical hydrography to provide time series of dynamic height profiles, which can then be differenced horizontally to give geostrophic velocities. The determination of the geostrophic velocities was done as follows: First historical hydrography was used to determine empirical characteristics relating subsurface temperature to specific volume anomalies (Meinen and Watts 2000); next the resulting profiles of specific volume anomaly were integrated vertically to give dynamic height anomalies relative to 1000 m; finally the time series of dynamic height anomalies were differenced either meridionally or zonally to give time series of geostrophic velocity profiles relative to 1000 m. The details of obtaining Ekman and geostrophic velocities are given elsewhere (Meinen and McPhaden 2001).

Meridional transports and velocities are calculated at 5°S and at 5°N between the TAO mooring longitudes (165°E, 180°, 170°W, 155°W, 140°W, 125°W, 110°W, and 95°W). Zonal transports are calculated across the longitudes of each of the lines of TAO moorings and are then integrated between 5°S and 5°N. The zonal transports calculated right on the equator, where the Coriolis parameter goes to zero and the Ekman and geostrophic relations break down, must be given special consideration. Variations in the frictional component of flow between 2°S and 2°N are neglected since these flows are very shallow and weak with very small transports relative to the geostrophic currents (McPhaden 1981; Picaut et al. 1989). The zonal component of the geostrophic velocity on the equator was estimated using

the meridionally differentiated form of the geostrophic approximation

$$\beta u = -\frac{\partial^2 \Delta D}{\partial y^2}, \quad (1)$$

where β, u, and ΔD represent the meridional derivative of the Coriolis parameter, zonal velocity, and dynamic height anomaly, respectively. This practice, often called equatorial geostrophy, has been shown to predict zonal flows fairly well given sufficient temporal and spatial sampling of the density field (Jerlov 1953; Arthur 1960; Hayes 1982; Lukas and Firing 1984; Bryden and Brady 1985; Picaut et al. 1989; Picaut and Tournier 1991). The second meridional derivative of ΔD is estimated from the second derivative of a parabola fit to the dynamic height values at 2°S, 1°S, 0°, 1°N, and 2°N. Picaut et al. (1989) compared the results from applying a similar second derivative method to the TAO buoys at 2°S, 0°, and 2°N (in their case mathematically equivalent to averaging the geostrophic estimates within 0°–2°N and 2°S–0°) to direct current meter measurements on the equator at 165°E and 110°W. Their results indicated that the variability of the zonal currents at seasonal and interannual timescales was well estimated using (1). They also indicated, however, that the long term mean zonal currents were not well determined by this method in all examined cases.

To correct for a mean bias in our transport estimates, the time series mean zonal geostrophic transport between 2°S and 2°N within a series of vertical layers was compared to mean absolute transports determined from a set of ship-mounted ADCP sections obtained by a number of programs (Johnson et al. 2001). At least nine ADCP sections were obtained along each TAO mooring line during the 1990s. The differences between the geostrophic values and the mean ADCP measured values were defined to be corrections for the mean geostrophic values; these corrections were determined both for transports above individual depth levels and above mean isotherm depths. The latter assumes the currents move up and down with the isotherms. Both corrections were calculated for a series of isotherms and depth levels as well as at a series of longitudes to document the zonal structure of the correction. The corrections range in magnitude from 2–3 Sv of westward flow in the upper 50 m at 170°W, where the magnitude of the South Equatorial Current has been underestimated by geostrophy, to about 30 Sv of eastward flow for a layer integrated down to 250 m at 125°W, where the Equatorial Undercurrent (EUC) magnitude has also been underestimated. Because these corrections derive from ADCP measurements, and hence are absolute velocities not geostrophic velocities, the corrections include other terms such as the mean frictional component of the velocities and the vertical Coriolis term (Joyce et al. 1988).

Ekman transports were assumed to be confined to the upper 50 m of the water column (Wyrtki 1981). Using one of the recent data-based models of the vertical structure of ageostrophic velocity (e.g., Ralph and Niiler 1999) might provide more near-surface structure. However, because the Ekman velocities are expected to be largest at the surface and to decrease significantly with increasing depth, the use of one of these models in the context of our experiment would probably not significantly change results below 50 m. No attempt was made to determine the vertical structure of the Ekman transport within the upper 50 m and no vertical velocities were calculated within the upper 50 m. The net horizontal transports in the upper 50 m were determined by combining the vertically integrated geostrophic transport within that layer (relative to a level of no motion at 1000 m) with the Ekman transport.

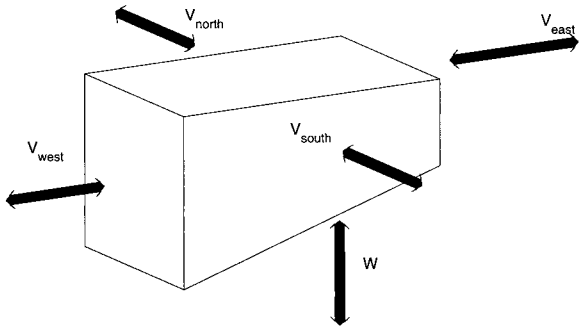

FIG. 2. Diagram of the terms in the volume balance used to estimate the vertical transport.

Included within W (total vertical transport) are both across and along isopycnal flows. With a diagnostic model of the equatorial Pacific, Bryden and Brady (1985) demonstrated that the W_{ci} (cross-isotherm vertical transport, which is roughly equivalent to the cross-isopycnal flow in this region) is much smaller than W. Both W and W_{ci} were determined as part of this study. The estimation of W across a depth level assumed both that volume is conserved in a box and that the volume transport through the ocean surface is negligible (Fig. 2). If the bottom of the box is defined to be a depth surface, then

$$W = V_{\text{north}} + V_{\text{east}} - V_{\text{south}} - V_{\text{west}}, \quad (2)$$

where W denotes the vertical transport across the base of the box, V denotes a horizontal volume transport integrated above the box base, and the subscripts denote the sides of the box. The signs of the terms arise from defining northward, eastward, and upward transports to be positive. The transports across the four sides of the box each have both Ekman and geostrophic components. The depth level used for the bottom of the box can vary, the only difference being the vertical range over which the geostrophic transports are integrated, so W can be estimated at a range of depths. Note, however, that the 50-m Ekman layer depth is the shallowest level that can be used for the base of the box. For this study W was determined across depth levels at 10-m intervals ranging

from 50 m to 1000 m. As mentioned earlier, the zonal transports were integrated between 5°S and 5°N, while the meridional transports were integrated separately between pairs of TAO lines ranging from 165°E to 95°W. This gives seven boxes along the equator, each spanning 5°S–5°N and all but one spanning 15° of longitude. (The exception spans only 10° of longitude between the date line and 170°W.)

If the base of the box in Fig. 2 is, instead, defined as a temperature surface and the horizontal transports are integrated from the sea surface down to that temperature surface, then it is possible to estimate the component of the transport across the isothermal surface, W_{ci}. The important thing to keep in mind is that this represents a volume balance in a box with a moving bottom, where the bottom moves as the isotherm in question moves up and down. Here W_{ci} is given by

$$W_{ci} = \frac{\partial B}{\partial t} + \mathcal{V}_{\text{north}} + \mathcal{V}_{\text{east}} - \mathcal{V}_{\text{south}} - \mathcal{V}_{\text{west}}, \quad (3)$$

where B denotes the volume of water in the box, $\mathcal{V}$ denotes a horizontal volume transport integrated above a particular isotherm surface, and the subscripts denoting the sides of the box. Again the horizontal volume transports have both Ekman and geostrophic components. B is calculated using the monthly BMRC subsurface temperature data and $\partial B/\partial t$ is determined as the centered differences between these monthly values. This calculation can be done for a series of different isotherms simply by looking at the transports of water warmer than that isotherm across the four horizontal sides and the changes in the depth of that isotherm. Again, because of the assumption of an Ekman layer 50 m deep, the bottom of the box must be at least as cold as the coldest temperature observed at 50 m.

The W_{ci} calculated from (3) is more than simply $W\cos(\theta)$, where θ is the angle the isotherm surface makes with horizontal, because the horizontal velocities can have cross-isotherm components and so must also be considered. If the isotherm slopes upward to the east (i.e., no meridional slope) then $W_{ci} = W\cos(\theta) - U\sin(\theta)$ where U is the zonal transport. Estimates of W_{ci} calculated using this latter method are similar to the results of (3). However, for the results shown hereafter the method employing (3) is used because it is simpler to implement and requires fewer assumptions.

Estimates of w (total vertical velocity) and w_{ci} (cross-isotherm vertical velocity) can be derived from W and W_{ci} simply by dividing by the horizontal area of the box. The lack of meridional resolution, however, means that the vertical velocities obtained are averages across 5°S to 5°N, as well as across the zonal range of each box. Higher meridional resolution would be desirable through this latitude band, given the meridional structure of zonal currents. As already mentioned, however, the determination of meridional velocities through geostrophic and Ekman dynamics limits our results to averages between 5°S and 5°N. Repeat ADCP sections, while noisy, suggest that in the time mean the upper 100 m between 4°S and 5°N is dominated by upwelling (Johnson et al. 2001). The more abundant surface drifter data, however, suggest that mean equatorial surface divergence may be confined between 2°S and 2°N, with smaller surface convergences flanking the equator between 2° and 8° latitude (Johnson 2001). This structure cannot be resolved here.

4. Results

This section presents the vertical transports and velocities, and is organized into three subsections: a presentation of the horizontal divergence above 50 m and 150 m; a presentation of the total vertical velocity (w) and the cross-isotherm vertical velocity (w_{ci}) as a function of longitude and time across the basin; and a presentation of w and w_{ci} spatially averaged over the eastern portion of our study area under the ''Cold Tongue,'' a region of anomalously cold SSTs along the equator in the eastern Pacific (Philander 1990). Each subsection is organized into a discussion first of the time mean, then of the variability. The section ends with comparisons with historical estimates. As noted earlier only results using ECMWF winds are shown; root-mean-square differences with results using other wind products were about 0.10×10^{-5} m s^{-1} (roughly 10%–30% of the peak-to-peak vertical velocity signal in each small box).

a. Horizontal velocity structure and divergence

While the zonal and meridional geostrophic velocities were calculated relative to a level of no motion at 1000 dbar, the majority of the vertical shear in the horizontal velocities was found between the surface and 300 m (Fig. 3). Both the zonal and meridional transport components indirectly provide evidence of vertical motion. The shoaling of the eastward flowing EUC toward the east necessitates some vertical motion. Also, in the meridional direction the geostrophic convergence towards the equator occurs over the upper 200 m, while the Ekman divergence (not shown) is expected to occur in a much shallower layer, for the purposes of this study above 50 m. This difference in depth ranges necessitates vertical motion to complete these meridional circulation cells based on mass conservation.

The contribution of the geostrophic and Ekman transports to the horizontal divergence in the upper 50 m within 5°S–5°N, 165°E–95°W was calculated for the period January 1993 through September 1999 (Fig. 4). The geostrophic convergence was broken into zonal and meridional components. The divergence due to the zonal Ekman transports was so small that only the full Ekman divergence is plotted, noting that it is strongly dominated by the meridional component.

The Ekman transports are by far the largest compo-

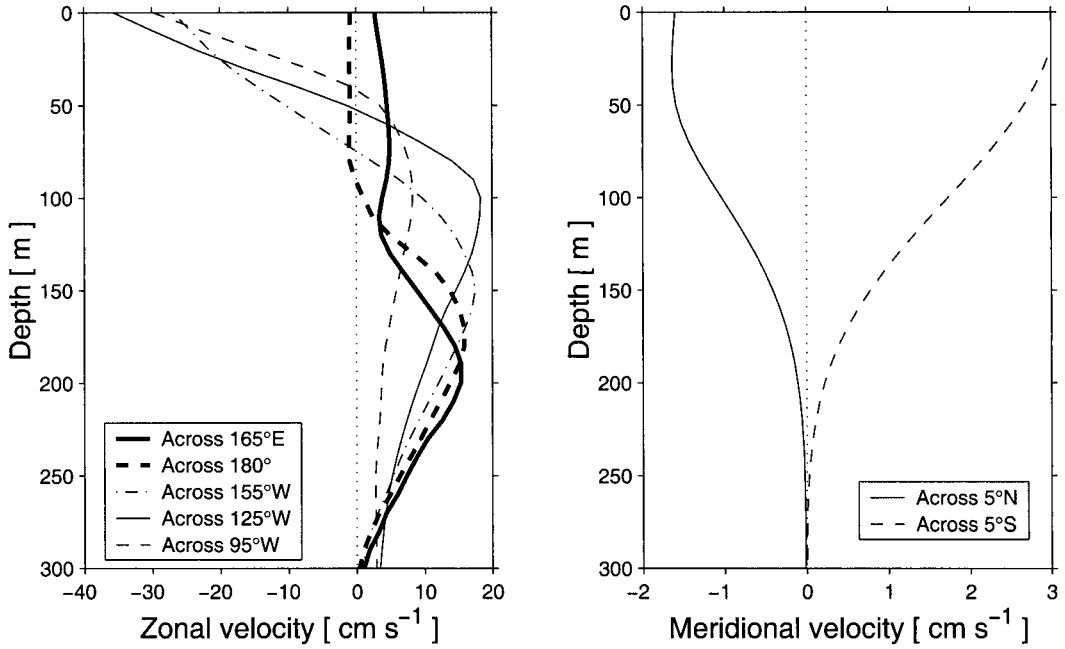

FIG. 3. Mean horizontal geostrophic velocity profiles during 1993–96 (relative to a level of no motion at 1000 m). Zonal velocities (left panel) are averaged between 5°S and 5°N and are across the longitudes indicated in the legend. Meridional velocities (right panel) are averaged between 165°E and 95°W and are across the latitudes indicated in the legend. Zonal velocities between 2°S and 2°N were corrected using the ADCP measurements described in the text prior to the meridional averaging, and hence include a portion of the directly wind-forced mean flows.

nents of the mean horizontal divergence above 50 m, discharging on average about 60 Sv of warm near-surface water towards the poles (bold tick marks on right axis of the upper panel of Fig. 4 show the 1993–96 mean values of the divergence components). The mean meridional geostrophic convergence in the upper 50 m counteracts around half of the Ekman divergence while the mean zonal geostrophic convergence plays a much smaller role in the mean total divergence. The mean total horizontal divergence above 50 m from the region within 5°S–5°N, 165°E–95°W was about 30 Sv. Because volume must be conserved, this mean total horizontal divergence must be balanced by an equivalent upwelling across 50 m. This corresponds to a spatially averaged temporal mean upwelling velocity of about 0.24×10^{-5} m s^{-1} $\pm$ 0.02×10^{-5} m s^{-1} (see appendix for discussion of error estimate).

Variability of the total horizontal divergence above 50 m (and hence W across 50 m) is largely controlled by meridional Ekman divergence (Fig. 4, lower panel). The total divergence and Ekman divergence agree in magnitude and phase, and both exhibit prominent annual and semiannual cycles. In addition, there is a significant annual cycle to the zonal geostrophic convergence that contributes to the total divergence. At interannual time scales the dominant variability appears to be in the meridional geostrophic and Ekman transports (Fig. 4, upper panel), with the signals in both during the 1997–98 El Niño event exceeding the corresponding signal in the zonal geostrophic convergence.

Integrating the divergence downward from the surface to 150 m gives a different picture (Fig. 5). In the layer above 150 m the mean meridional Ekman divergence nearly matches the mean meridional geostrophic convergence in magnitude (again, bold tick marks on right axis of the upper panel of Fig. 5 show the 1993–96 mean values of the divergence components). The mean total horizontal divergence and the zonal geostrophic convergence have nearly equal mean values of approximately zero (bold ticks overlay one another in Fig. 5). At seasonal timescales the zonal geostrophic divergence variability has over twice the peak-to-peak amplitude of the Ekman and meridional geostrophic signals (Fig. 5, lower panel). These seasonal variations in zonal geostrophic convergence, like those over the shallower 0–50 m layer, are associated with wind-forced low baroclinic mode equatorial Kelvin and Rossby waves (see, e.g., Fig. 13 of Yu and McPhaden 1999). The greater prominence of the zonal geostrophic convergence in the upper 150 m vis-à-vis the upper 50 m on seasonal timescales is consistent with greater depth scale of these waves compared to the depth scale for Ekman flows. The increase in magnitude of zonal geostrophic convergence between the upper 50 m and upper 150 m on interannual time scales (cf. Figs. 4 and 5, upper panels) is also consistent with the vertical coherence of low baroclinic mode equatorial waves. At interannual timescales, there is a tendency for meridional Ekman divergence and geostrophic convergence to balance one another over the upper 150 m (Fig. 5, upper

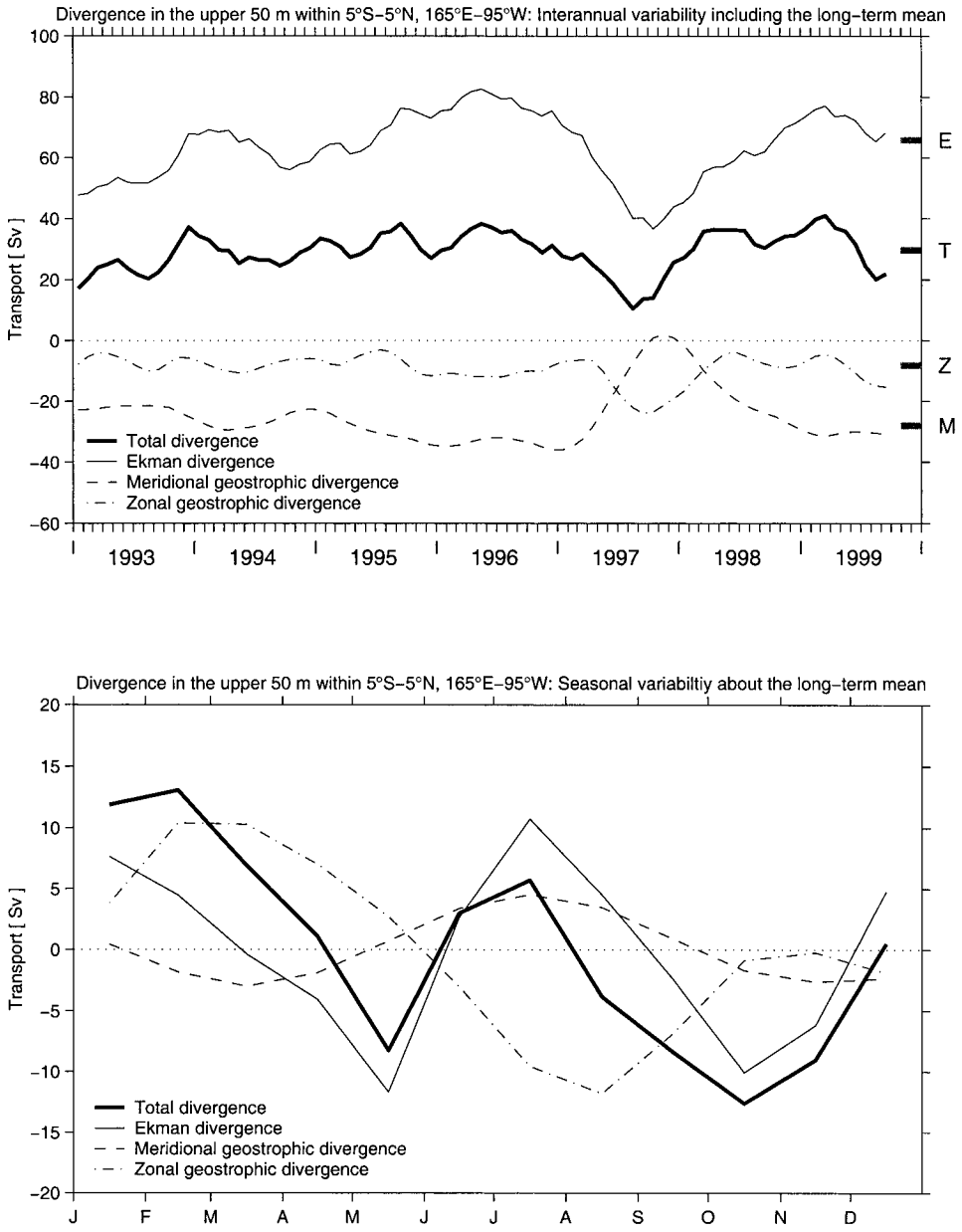

FIG. 4. Divergence in the upper 50 m within 5°S–5°N, 165°E–95°W for 1993–99. Upper panel: Interannual variability after removal of seasonal signal (but still including time series mean). Lower panel: Seasonal variability. Positive values indicates flow out of the box. Mean values of the total horizontal divergence (Ekman plus geostrophic), Ekman divergence (including both zonal and meridional Ekman divergence however meridional strongly dominates), meridional geostrophic divergence, and zonal geostrophic divergence are indicated by bold ticks on right axis of upper panel with the labels T, E, M, and Z, respectively. Divergence is measured in Sverdrups [Sv $\equiv 10^6$ m^3 s^{-1}].

panel). This indicates that over the seven-year period, the shallow meridional overturning circulation in the interior ocean tends to be confined above 150 m. The balance is not perfect though, particularly during 1997–99 when there were major equatorial wave induced vertical displacements of the thermocline extending to 150 m associated with the 1997–98 El Niño and 1998–99 La Niña (McPhaden and Yu 1999).

Wyrtki (1981) suggested that the majority of the zonal convergence/divergence for the equatorial Pacific was below 50 m within the EUC. Our results indicate a significant mean (1993–96) zonal convergence (~6 Sv) within the layer above 50 m, demonstrating that not all of the zonal convergence is confined to the EUC. In fact, integrated down to 150 m the mean zonal convergence is nearly zero, indicating the zonal convergence

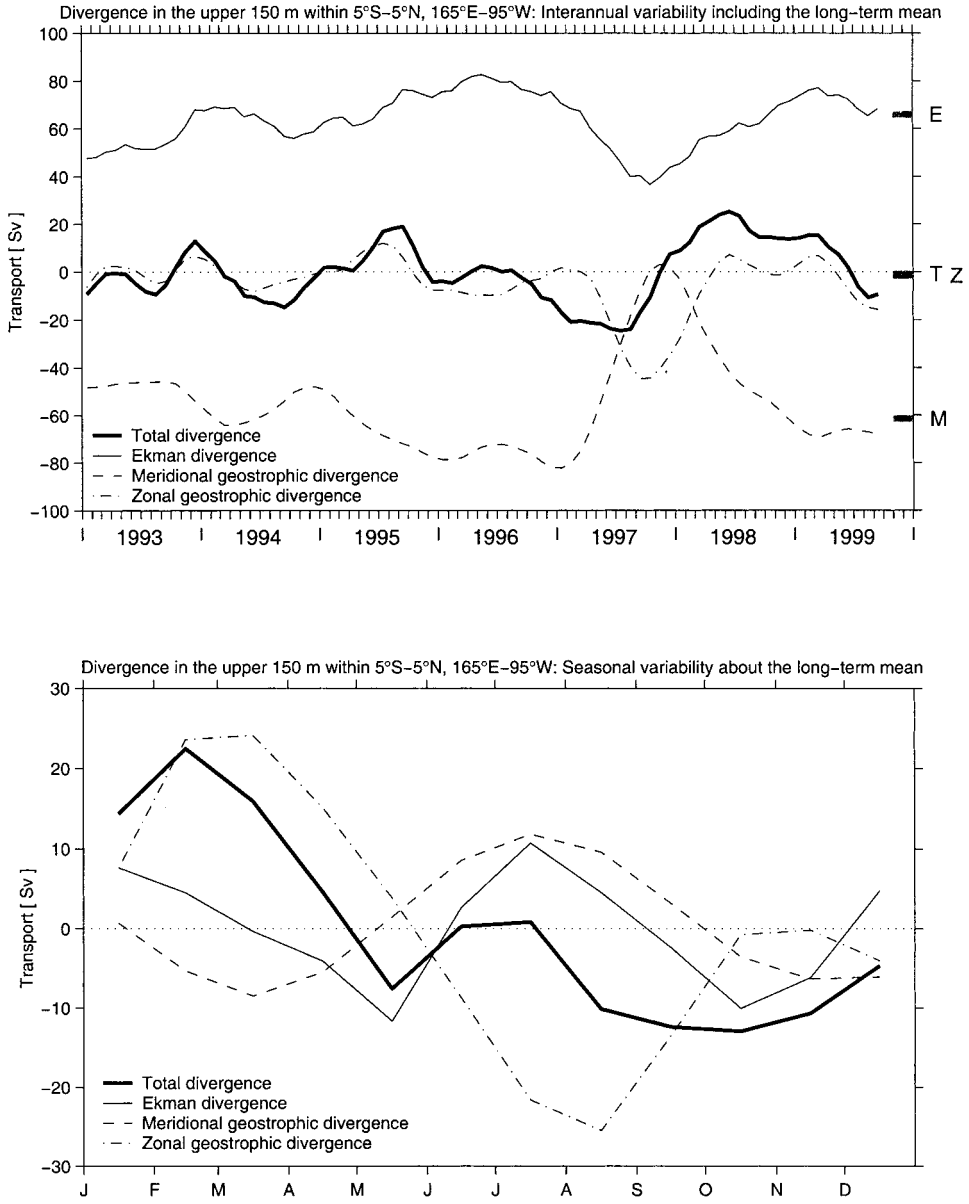

FIG. 5. Divergence integrated over upper 150 m. Details follow Fig. 4.

above 50 m is counteracted by a zonal divergence between 50 and 150 m.

b. Vertical velocity and transport as a function of longitude and time

The mean vertical structure of the total vertical velocity (w) along the equator tends to follow the thermocline structure and the mean τ_x (Fig. 6, middle and upper panels). The peak upwelling at 50 m coincides fairly well with the strongest westward winds, offset by about 15° longitude. The mean w decreases with increasing depth and tends to change sign below the main thermocline. It should be kept in mind, however, that the error bars on w increase with increasing depth (see appendix). At 200 m the estimated accuracy of the mean w averaged over 15° of longitude is $\pm$ 0.28 $\times$ 10^{-5} m s^{-1}, indicating that below about 200 m the w estimates are not statistically meaningful. Further, the error estimates quoted here are estimates of the measurement errors and do not include the standard error of the mean (SEM) since the SEM would vary for each box in which w was estimated. The SEM was determined at each longitude and depth where w was determined; for the mean values of w shown here the SEM never exceeded 0.16 $\times$ 10^{-5} m s^{-1} above 200 m and were never large enough to significantly increase the total estimated error bar (defined as the square root of the sum of the squares

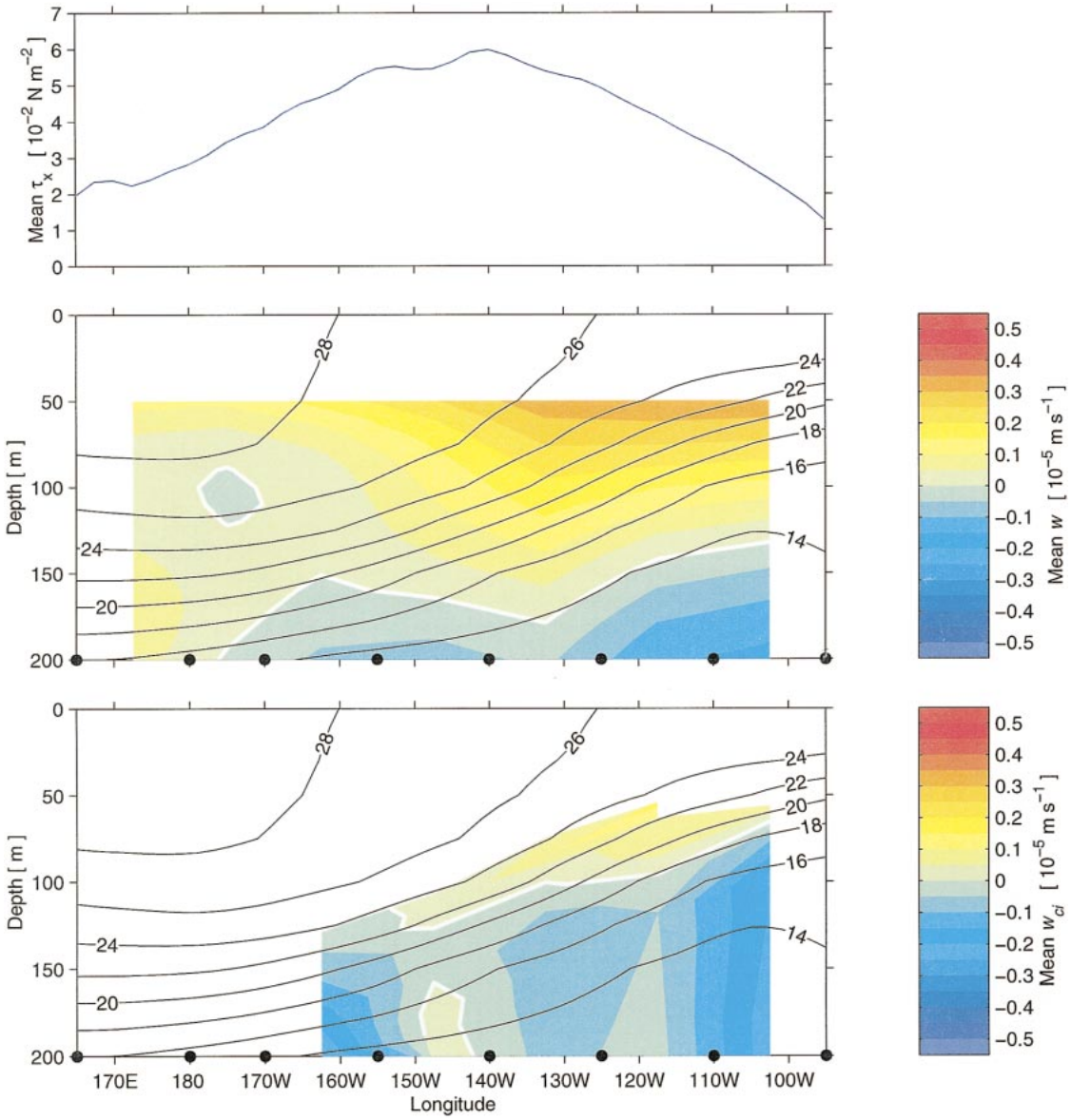

FIG. 6. Mean (1993–96) section of vertical velocities w (middle panel) and w_{ci} (lower panel) averaged 5°S–5°N. Colors denote w, white contours denote zero w, black line contours show mean temperature section at 2°C intervals. Both w and w_{ci} have been smoothed zonally with a three-point running mean to eliminate vertical banding features which result from the vertical integration of the volume budget. Bold dots denote TAO array longitudes. Blank regions in the bottom panel denote regions where w_{ci} wasn't calculated (isotherms above 24°C), regions where the isotherms rose above 50-m depth (and hence contacted the base of our Ekman layer), or regions where the standard error of the mean was large enough to indicate the calculated means were not robust. Upper panel shows temporal mean zonal wind averaged along 5°S and 5°N. Positive wind stress indicates westward flow.

of the SEM and the measurement errors). At greater depths, however, the SEM became comparable to or larger than the measurement error estimates. The tendency for negative w below the main thermocline has been observed in other studies (Bryden and Brady 1985; Weisberg and Qiao 2000), however, which gives some confidence in the observed trend. A later section will present a more complete discussion of comparisons with historical estimates of w.

As discussed earlier, (3) was used to determine the cross-isotherm component of the vertical velocity, w_{ci} (Fig. 6, lower panel). The calculation of w_{ci} was somewhat noisier than for w because (3) involves additional variability (due to the rate of change of volume above each isotherm surface). The SEM was determined for the w_{ci} values as well, and regions where the SEM was higher than 0.20×10^{-5} m s^{-1} were defined to be regions wherein the mean value could not be accurately determined using the four-year time series. This cutoff was chosen because this value is comparable in mag-

nitude to the estimated measurement accuracy and thus the error bars estimated in the appendix would significantly underestimate the true error about the mean for SEM greater than the cutoff. Values of the SEM larger than this cutoff occurred only for w_{ci} estimates west of 170°W, collocated with the largest variations in the Ekman transports and the largest zonal geostrophic velocity variations.

The temporal mean structure of w_{ci} (Fig. 6, lower panel) has some similarities to the structure of w (Fig. 6, middle panel), with upward flow at shallower depths in the eastern Pacific and a transition to downward flow occurring near the middle of the main thermocline. The transition between upward and downward flow in the eastern Pacific was shallower for w_{ci} than it was for w. This difference is statistically significant and it has implications for how the vertical advection term impacts the overall heat budget.

The east–west structure of w and w_{ci} was fairly similar, with the strongest upward velocities occurring near the location of the peak westward winds (and hence the strongest meridional Ekman divergence). For both w and w_{ci} the peak upwelling occurred slightly east of the peak in τ_x, although for w_{ci} this peak location was difficult to determine for certain since the 24°C was the warmest isotherm used for the calculation of w_{ci}. In general, for both w and w_{ci} the mean vertical velocities trend from upwelling near 50 m to downwelling at 200 m.

Throughout the basin the temporal variability in w and w_{ci} was fairly coherent in the vertical although the amplitude of the variability did exhibit some changes with depth. Furthermore the variations in w_{ci} were generally consistent with, but of smaller amplitude than, the variations in w. Because of these structural similarities between w and w_{ci} and their vertical coherences, we document only the variability of w at a depth of 50 m.

Most of the time w at 50 m was positive (upwelling) though there was significant zonal and temporal variability around the mean (Fig. 7, upper panel). In order to study this variability in greater detail at different timescales, seasonal cycles of both w and τ_x were estimated using the data from 1993–96 (Fig. 7, middle panel). Interestingly, both the τ_x and w signals include a prominent semiannual component with westward wind anomalies in boreal winter and summer, and eastward wind anomalies during boreal spring and fall. There is a corresponding pattern in w, with upwelling anomalies corresponding to westward wind anomalies and downwelling anomalies corresponding to eastward wind anomalies. The seasonal variations in w have a peak-to-peak amplitude of about 0.40×10^{-5} m s^{-1}. In the eastern part of the basin, w at 50 m shows the largest positive seasonal anomalies in January and February, with a secondary maximum in July and August. The largest negative anomalies occur during April and May, with a secondary maximum in September and October. At seasonal timescales the correspondence between τ_x and w is very good, but not perfect. We expect that remotely forced Rossby and Kelvin waves may be important at both annual and semiannual periods (Meyers 1979; Busalacchi and O'Brien 1980; Yu and McPhaden 1999). Nevertheless, the correspondence between the local τ_x and w suggests that local wind forcing is playing a dominant role. This agreement with the winds is consistent with the divergence plot (Fig. 4, lower panel), which showed the seasonal Ekman variability to be the largest component of, and to be in phase with, the total horizontal divergence.

Poulain (1993) also found a semiannual signal in his estimates of upwelling. However, he showed maximum positive w anomalies across 50 m during April through June, with a secondary maximum in October and November, and maximum negative anomalies during February and March, with a secondary maximum in August. It should be remembered, however, that the results of Poulain (1993) represent a w averaged over only 1°S–1°N, while our results refer to velocities averaged over 5°S–5°N. This difference in meridional averaging scales could be one reason for the observed differences between results. Kessler et al. (1998) presented an ocean general circulation model estimate of the seasonal signal in w near the equator at 110°W. The model seasonal cycle showed no semiannual signal for the upwelling. However, the seasonal cycle of wind stress forcing in that study was based on FSU winds for the period 1961–90, during which there was apparently a less pronounced semiannual signal. All three wind products tested for this study (ECMWF, FSU, and SCAT) exhibited a semiannual signal when averaged along 5°S and 5°N for the period 1993–96.

Removing the mean seasonal cycle as well as the four year (1993–96) mean highlights the interannual variability (Fig. 7, bottom panel). As with the seasonal variations, there is a tendency for the upwelling anomalies to be associated with anomalous westward winds and downwelling anomalies to be associated with anomalous eastward winds. The relationship is not quite as clean as for the seasonal cycle, especially during the early part of the record (1993–95) when the wind and w anomalies are small. The best agreement between the phasing of τ_x and w occurs in the western part of the study region during the 1995–96 La Niña, the 1997–98 El Niña, and the 1998–99 La Niña. Interannual variability of τ_x and w in the western part of our region is correlated at the 95% significance level, with τ_x leading by 1–9 months. This indicates that the local τ_x variability results in a strong response in w, although the broadness of the correlation peak indicates that nonlocally forced Rossby and Kelvin waves must also be playing a significant role in the w variability (Boulanger and Menkes 1999; McPhaden and Yu 1999). In the eastern part of the basin, correlations are not statistically different from zero at the 95% level for any lag, which may be due to the small magnitude of the τ_x variability in the east and to the relatively large influence of remotely forced equatorial waves.

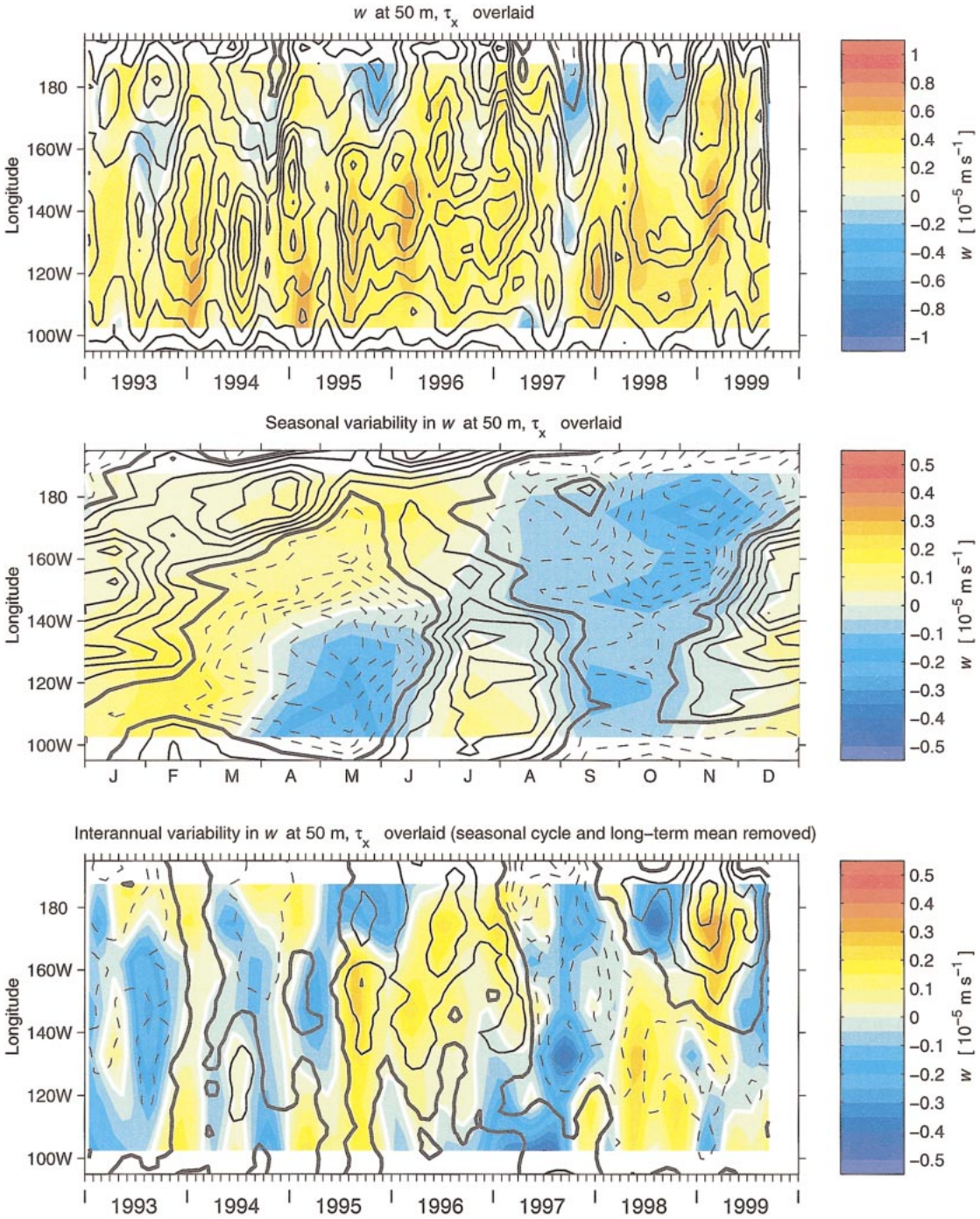

FIG. 7. Zonal wind stress τ_x and vertical velocity w at 50-m depth. The τ_x are averaged at 5°S and 5°N. The w represent an average over 5°S–5°N and over 10°–15° of longitude; raw monthly estimates are accurate to within $\pm 0.32 \times 10^{-5}$ m s^{-1} and seasonal signals are accurate to within $\pm 0.18 \times 10^{-5}$ m s^{-1} (see appendix). Color shading denotes w, white line denotes zero w. Solid black contours indicate westward τ_x (or westward anomalies), dashed black contours denote eastward τ_x (or eastward anomalies). Contour interval for winds is 0.01 N m^{-2} on upper two panels, 0.0025 N m^{-2} on lower panel, with bold line indicating zero. Top panel shows full w and τ_x, middle panel shows the 1993–96 seasonal cycle, bottom panel shows interannual variability after the removal of the seasonal cycle and the 1993–96 mean. Note that color contour interval on middle and lower panel is half that of color contours on top panel.

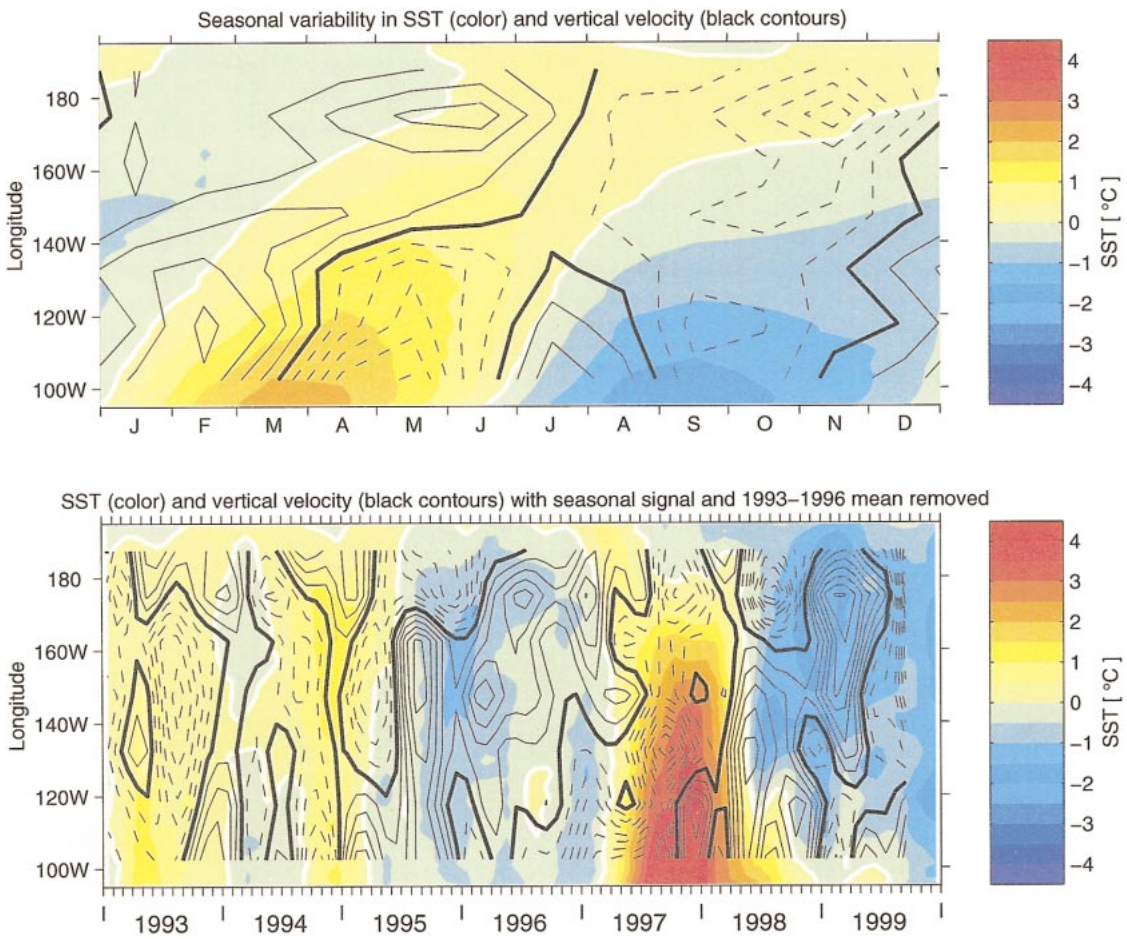

FIG. 8. Reynolds SST anomaly averaged between 5°S and 5°N as a function of longitude and time. Zero SST anomaly is indicated by white contour. Vertical velocity overlaid as black contours; solid contours denote upwelling tendencies, dashed contours denote downwelling tendencies. Top panel shows the 1993–96 mean seasonal cycle, bottom panel shows interannual variability after the removal of the seasonal cycle and the 1993–96 mean.

An interesting comparison can be made between w at 50 m and the SST (Fig. 8). At interannual timescales, there tends to be a negative correlation between the SST and w at 50 m (Fig. 8, bottom panel). Throughout the time series there is a tendency for upwelling coincident with cold SSTs and vice versa, especially in the central and eastern equatorial Pacific. This tendency is consistent with the expectation that upwelling of cold, deeper waters will cool the SST, while downwelling isolates the surface from the deep cold waters and warm SST anomalies can form due to the other terms in the heat balance. This correspondence is least apparent in the west where the waters roughly between 100 m and 50 m are of nearly the same temperature as those above 50 m due to the deep thermocline (Philander 1990). As such vertical advection would have less effect on the surface heat balance and hence the SST in the western part of our region. The agreement between SST and w is hardly exact even in the east, however, as should be expected since $w\partial T/\partial z$ is only one part of the surface layer temperature balance (Wang and McPhaden 1999; Wang and McPhaden 2000). Furthermore, the temperature balance indicates that in fact it is the temporal derivative of SST, which should correspond to $w\partial T/\partial z$, so some phase lags are to be expected between SST and w. At seasonal timescales the agreement between the SST and w (Fig. 8, top panel) is poor even considering a phase lag. A marked semiannual signal exists in w, while there is no equally strong semiannual cycle in the SST. This suggests that the $w\partial T/\partial z$ term in the surface layer heat budget may not be playing a dominant role at seasonal timescales, although the disparity could also result from some combination of the other terms in the heat budget obscuring the signal due to vertical advection. As noted above, the vertical advection term does seem to play a significant role at interannual timescales.

c. Vertical velocity in eastern equatorial Pacific

There is considerable interest in quantifying the magnitude of the vertical velocity in the eastern equatorial Pacific because of its impact on SST. For this reason,

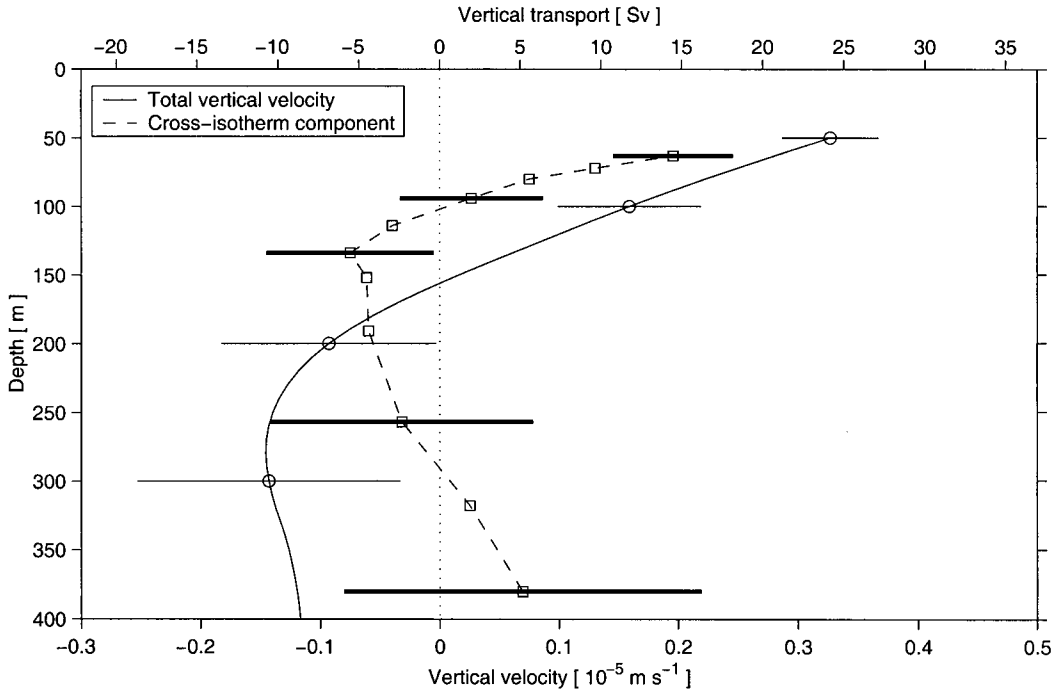

FIG. 9. Mean (1993–96) profiles of vertical velocity and transport integrated within 5°S–5°N, 155°–95°W. Both the total vertical velocity (w, solid line) and cross-isothermal vertical velocity (w_{ci}, dashed line) are shown. The w_{ci} are plotted at the mean depth of isotherms within this region. Isotherms used (denoted by squares) are 10°, 11°, 12°, 13°, 14°, 15°, 17°, 20°, 22°, 23°, and 24°C. Error bars indicating estimates of the accuracy of the total vertical velocity are plotted at four representative levels (denoted by circles), as are error bars for the cross-isothermal vertical velocity at five isotherm levels.

w and w_{ci} were integrated over the ''Cold Tongue'' region, defined in this study as being within 5°S–5°N, 155°–95°W. The mean vertical profile of w for this region indicates upwelling above about 160 m and downwelling below (Fig. 9). The latter is statistically different from zero based on the estimated accuracy of our w (including the SEM).

Averaged over this region, w_{ci} is much smaller than w (Fig. 9), as is expected based on earlier work (e.g., Bryden and Brady 1985). There is a trend in both w and w_{ci} to transition from positive values, or upwelling, above 100 m to negative values, or downwelling, below. While the estimated error bars become quite large below 200 m, because of the vertical integration of errors in the horizontal divergence, there is a tendency for both w_{ci} and w to approach zero below 250 m. As discussed earlier the upper meridional circulation cells were generally contained above 150 m; the results in Fig. 9 suggest that the deeper meridional circulation cells must be confined to between 150 m and 400–500 m in the interior equatorial Pacific ocean (i.e., away from the western boundary currents).

The sign change in w_{ci} occurs about 60 m shallower than for w, consistent with earlier studies (Bryden and Brady 1985; Weisberg and Qiao 2000). The transition from positive w_{ci} to negative w_{ci} demarcates the layers in this region where, on average during 1993–96, layers were either gaining heat or losing heat. At a depth where w_{ci} is positive, waters that were below the local isotherm are moving upward across the isotherm and are hence becoming warmer. At a depth where w_{ci} is negative, waters that were above the local isotherm are moving downward across the isotherm and are hence becoming colder. Warming or cooling occurring in a time-mean sense does not violate the conservation of heat because the waters in these regions do not stay in these regions; they regularly move out of the equatorial band toward the poles and then return after modification by mixing and air–sea interaction at higher latitudes. The mean profile of w_{ci} therefore indicates that in this region waters above 105 m are being warmed on average while waters below 105 m and above about 300 m are being cooled on average.

Vertical heat advection by w is one term in the heat balance for any particular layer. However the mean profile of w for this region has a significantly deeper zero-crossing (160 m), indicating that net heating and cooling determined from the w_{ci} profile is not solely due to the vertical advection term. A complete heat balance is beyond the scope of this paper. Nonetheless, these results do indicate that the horizontal advection, horizontal mixing, and net surface heat flux terms must be combining to play a role in the heat balance at least comparable to that played by the vertical advection.

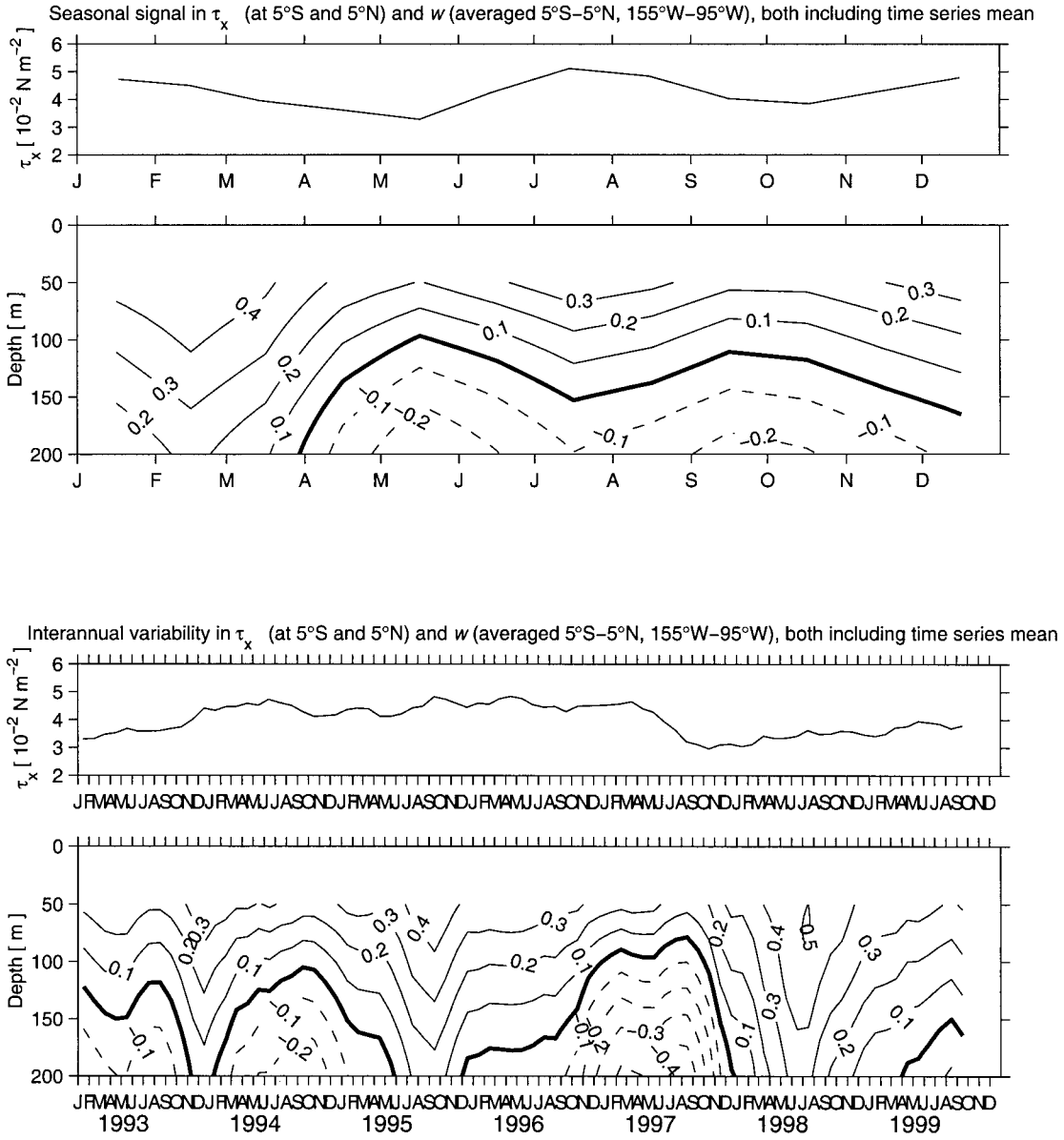

FIG. 10. Time series of w and τ_x in the ''Cold Tongue'' region. The τ_x are averaged within 155°–95°W along both 5°S and 5°N, and the resulting means at 5°S and 5°N are then averaged with each other. Positive τ_x indicate westward winds. The w represent an average over 5°S–5°N, 155°–95°W. Upper two panels: Seasonal cycles in τ_x and w, respectively, both determined over 1993–96 and including the 1993–96 mean. Lower two panels: τ_x and w, respectively, after the removal of the seasonal cycle (but still including the 1993–96 mean).

The time series of the spatially averaged w anomalies for the ''Cold Tongue'' region shows obvious seasonal and interannual signals (Fig. 10). The correspondence between the seasonal signal in τ_x and w at 50 m mentioned earlier is quite apparent, and the peak-to-peak amplitudes of the seasonal w signal (Fig. 10, upper panel) are nearly as large as the peak-to-peak amplitudes of the interannual signal during the 1997–98 El Niño event (Fig. 10, lower panel). The poor correspondence mentioned earlier between the interannual signal in τ_x and the interannual signal in w across 50 m is shown more dramatically here, with large variations in w occurring in late 1993, mid 1995, and all of 1998 with little or no corresponding signal in τ_x. This highlights the importance of Kelvin and Rossby waves to the vertical velocity signals in the ''Cold Tongue'' region on interannual timescales.

d. Comparison to historical vertical velocity estimates

For the purposes of this paper, historical w estimates in the equatorial Pacific can be broken up into three categories: those which determine W (vertical transport)

estimates over a region (e.g., Wyrtki 1981; Quay et al. 1983; Bryden and Brady 1985; Poulain 1993; Johnson and Luther 1994; Johnson et al. 2001); those which determine w (vertical velocity) at a point directly on the equator (e.g., Halpern and Freitag 1987; Halpern et al. 1989; Qiao and Weisberg 1997; Weisberg and Qiao 2000); and those which determine vertical boundaries for w based on tracers but do not make W or w estimates (e.g., Wyrtki and Eldin 1982; Fine et al. 1983). The first kind of study presents the best opportunities for comparison against our results. Only those studies which spanned the same range of latitudes can be directly compared to our estimates because of the considerable meridional structure in w between the equator and 5°S and 5°N (Johnson and Luther 1994; Johnson et al. 2001). Furthermore, most of the historical studies did not address seasonal or interannual variability, so this comparison must focus on the temporal mean. Finally, nearly all of these studies focused on the central and eastern portion of the equatorial Pacific; thus we present a comparison of profiles of w in the eastern equatorial Pacific (Fig. 11). As these historical studies each determined a W over essentially the same latitudinal range (5°S–5°N) but over slightly different longitudinal ranges, the historical estimates have been adjusted to account for the different regional surface areas by scaling up (for those which used smaller zonal ranges) or down (for those which used larger zonal ranges) by the ratio of the surface areas. With one exception [the results of Johnson et al. (2001)] the area adjusted results generally agree quite well for both W (upper panel, Fig. 11) and W_{ci} (lower panel, Fig. 11).

Quay et al. (1983) used historical hydrography to develop a two-dimensional budget for bomb ^{14}C distributions, and their estimate for the W at the base of the 50-m mixed layer of 26 $\pm$ 7 Sv (scaled to correspond to our region) agrees well with our mean result of 24 $\pm$ 3 Sv. The Quay et al. (1983) study only published an error bar for the 50-m w estimate, not their deeper estimates, and the Wyrtki (1981) and Bryden and Brady (1985) estimates did not provide error estimates. The Johnson et al. (2001) estimate of W at 50 m (57 $\pm$ 16 Sv) is significantly larger than for any of the other studies. Johnson et al. (2001) used repeated shipboard-ADCP transects to develop a set of mean horizontal velocity estimates and then used these horizontal velocities and the equation of continuity to determine w as a function of latitude and depth averaged longitudinally over 170°W to 95°W. In contrast to the other regional studies, Johnson et al. (2001) used direct velocity measurements, not geostrophic and Ekman dynamics-based estimates. As noted in that study, however, the direct velocity measurements were quite noisy, which may help to explain the significant difference from the other studies shown in Fig. 11. Furthermore, Johnson et al. (2001) included data from during the strong 1997–98 El Niño and 1998–99 La Niña events in developing their mean w estimates; Figs. 7 and 10 indicate significant interannual variations in w during those events so by including 1997–99 in the calculation of the mean they may have biased their estimated mean value.

The historical studies which provided point estimates of w on the equator cannot be directly compared against our w estimates, nor can those studies which only provided vertical boundaries for the upwelling. The vertical structure of the profiles, however, can be compared. Weisberg and Qiao (2000) determined that the transition from upwelling to downwelling was near 140 m, approximately at the core of the EUC, while Halpern and Freitag (1987) found it near 160 m, and Bryden and Brady (1985) found the zero crossing at about 180 m. Quay et al. (1983) determined the zero crossing to be at 225 m at 155°W based on the tracer pattern, roughly consistent with the results shown in Fig. 6. Fine et al. (1983) found the zero crossing at the depth of the 16°C isotherm, about 200 m in their data, based on the tritium signal. Our study found the zero-crossing at about 160 m, in the midrange of these other estimates. The distinction between these various depths may be simply due to noise in the estimates since the determination of w is quite noisy from all of these methods. The disagreement could also be due to the fact that the various volume balance estimates of w [ours along with Quay et al. (1983) and Bryden and Brady (1985)] represent an average over 5°S–5°N, while the estimates of Weisberg and Qiao (2000) are point measurements directly on the equator. Because the EUC is tightly confined along the equator (Johnson et al. 2001), an average over 5°S–5°N may not be well suited to determining the zero-crossing of w within the EUC. On the other hand, the differences (if real) may be significant for both dynamical and material property balances (Weisberg and Qiao 2000). Weisberg and Qiao (2000) argue that the transition to downwelling occurs at the core of the EUC, and thus significant downwelling is suggested in the lower part of the current, whereas these other studies, including our own, indicate that the downwelling is confined below the core of the EUC.

The agreement in vertical structure is better among the w_{ci} estimates. Weisberg and Qiao (2000), Bryden and Brady (1985), and our study indicate the transition from upward to downward w_{ci} occurs within 100–125 m, at or above the core of the EUC. This better agreement arises despite some differences in how the w_{ci} estimates were made [our study used a volume balance technique to obtain w_{ci} while both Bryden and Brady (1985) and Weisberg and Qiao (2000) used their w estimates in combination with the observed isotherm slopes]. As mentioned previously, tests with our data indicate the two different techniques result in estimates which are indistinguishable within our estimated error bars.

5. Summary and conclusions

This study has used geostrophic and Ekman transports calculated from observations of subsurface thermal

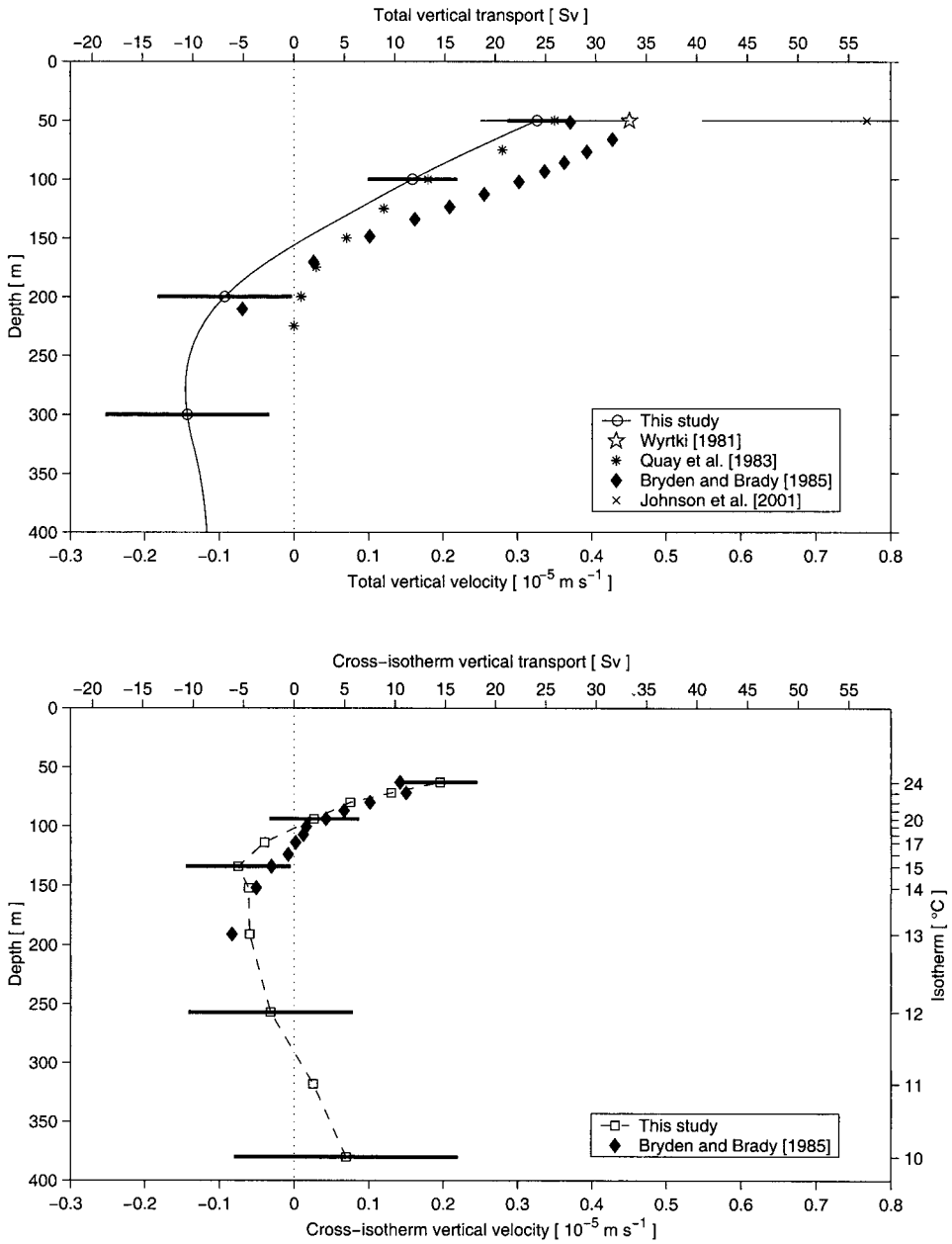

FIG. 11. Mean (1993–96) profiles of w averaged within 5°S–5°N, 155°–95°W. Both w (solid line, upper panel) and w_{ci} (dashed line, lower panel) are shown. Bold error bars indicate estimates of the accuracy. Estimates of w_{ci} are plotted at the mean depth of each isotherm used (noted on right axis) within this region. Also shown are historical estimates of vertical transports and velocities where the historical estimates have been scaled to compare directly to our region. Note that Bryden and Brady (1985) cross-isothermal transports have been plotted at the depths observed during our experiment, which varied by 10–15 m from the isotherm depths they observed. Thin error bars have been added to estimates that included published error bars.

structure and surface winds to determine vertical transports (W) and velocities (w) as a function of time, depth, and longitude in the equatorial Pacific within 5°S–5°N, 165°E–95°W during 1993–99 via a box volume estimate. The determination of W was in boxes of 10° of latitude by generally 15° in longitude and the corresponding w thus represents an average over these regions. The balance between meridional geostrophic and Ekman transports strongly dominates the total horizontal divergence in the upper 50 m averaged over 165°E–95°W at interannual timescales, while the zonal geostrophic convergence–divergence plays an important role at seasonal timescales. Integrating over the top 150 m shows that at interannual time scales the meridional

geostrophic and Ekman transports largely cancel one another during the weak El Niño and La Niña events during 1993–96, and as a result the variations of the total horizontal divergence reflect mainly changes in the zonal geostrophic convergence. During the large El Niño and La Niña events in 1997–99 the meridional divergence and zonal convergence played roughly equal roles in varying the total horizontal divergence above 150 m.

There is significant seasonal and interannual variability to the w signals in the equatorial Pacific. At seasonal timescales, w at 50 m is well correlated to the local winds. The same can be said for w at 50 m for interannual timescales in the western portion of our region, given a wind stress lead of 1–9 months, although the broadness of the correlation peak indicates that changes in w are also influenced by nonlocally forced equatorial waves. In the eastern portion of our region the relationship is less well defined on interannual time scales. The lack of a relationship between w and τ_x at interannual time scales in the east may imply that the variations in w in that region due to τ_x variations are being overwhelmed by the signals due to nonlocally forced waves.

The vertical structure of the mean w determined over 1993–96, a period chosen because of relatively weak interannual variability, shows upward flow within most of the Equatorial Undercurrent and above, with downwelling below, particularly in the eastern equatorial Pacific. The cross-isotherm component of the vertical velocity (w_{ci}) in the region 155°–95°W transitions from positive to negative near 105 m, about 60 m shallower than w. Our estimate for the mean W within 5°S–5°N compares well with the few historical box volume estimates which have been made even though the data used in those studies came from different decades (Wyrtki 1981; Quay et al. 1983; Bryden and Brady 1985). The basic structure of the vertical velocities, showing upwelling across the entire range of observed longitudes (165°E–95°W) at 50 m is consistent with previous modeling results (Philander et al. 1987).

While this study does not provide any information on the meridional structure of w, it does provide an observationally based look at the longitudinal structure of w and w_{ci}, as well as the seasonal and interannual variability of w. This information should be useful for not only physical oceanographic models of the equatorial Pacific circulation but also models of the near-surface biology and chemistry. The estimates made in this study also provide information on one of the most poorly known inputs to the upper-ocean heat budget, namely vertical velocity, and as such may improve future budget estimates. A future heat-budget analysis is planned over this same region to study the impact of vertical heat advection and the cross-isotherm component of vertical heat advection.

Acknowledgments. The authors would like to thank the following people for providing data used in this study: N. Smith, BMRC Australia, for the gridded subsurface temperature data; J. J. O'Brien and D. M. Legler at The Florida State University for the FSU wind pseudo-stress data; the European Centre for Medium-Range Weather Forecasts for the ECMWF wind data; R. Reynolds for the SST data; and IFREMER for the scatterometer wind data provided on the WOCE CD and the IFREMER Web site. William S. Kessler, Dana K. Savidge, Lynne D. Talley, and the anonymous reviewers all provided helpful suggestions on this manuscript. This project was funded by NOAA's Office of Global Programs and Environmental Research Laboratories as well as the Joint Institute for the Study of the Atmosphere and Ocean (JISAO) under NOAA Cooperative Agreement NA67RJO155.

APPENDIX

Accuracy of the Vertical Transport and Velocity Estimates

A detailed analysis of the errors in the geostrophic and Ekman transports used in this study, as well as the errors in the estimation of the volume of water above particular isotherms, has been presented elsewhere (Meinen and McPhaden 2001). Four distinct types of error that affected the estimated accuracy of the transports and volume, were discussed: instrumental, methodological, spatial sampling, and temporal sampling errors. Temporal sampling errors, quantified by determining the standard error of the mean (SEM), vary based on the time series in question and hence cannot be included in an error analysis that seeks to provide a single error estimate quantity calculated at several separate sites. The errors described in this appendix represent estimates of the instrumental, methodological, and spatial sampling errors, jointly referred to here as measurement errors. Within the text the SEM has been included where appropriate.

Ekman transport accuracy, which is difficult to quantify directly, was estimated by determining the root-mean-squared difference between the Ekman transports determined using the three different wind products as discussed in section 2. The largest error in determining the geostrophic transports relative to a level of no motion (no method was developed to quantify the error due to the level of no motion assumption used outside 2°S–2°N) results from variability in the temperature–salinity relationships used to convert the measured temperatures into dynamic heights. As such the geostrophic transport accuracies were determined by quantifying the errors that would be expected based on the observed temperature and salinity scatter in a large hydrographic database for this region and time period. Note that Meinen and McPhaden (2001) integrated the zonal transports across 8°S–8°N, whereas this study only used 5°S–5°N,

and that study also calculated meridional transports across 8°S and 8°N, whereas this study used 5°S and 5°N. Regardless of these distinctions, the error estimation techniques applied are identical. The resulting net horizontal transport error estimates based on the Meinen and McPhaden (2001) technique are used in this appendix to derive estimates for the accuracy of the vertical transports and velocities. Estimates are presented for the accuracy of the vertical velocity across 50 m, 200 m, and 20°C; other error bars discussed in the text were determined in the same manner.

The accuracy of the vertical transports is dependent on the spatial averaging region and thus must be quantified for the three separate size boxes discussed in this paper, each of which spans 5°S–5°N: boxes spanning 15° of longitude; a box spanning 60° of longitude; and the full region box spanning 100° of longitude. Regardless of which box size is used, the accuracy of the net zonal transport convergence is only a function of the vertical integration range since all three box sizes have the same meridional range. The size of the net meridional transport convergence errors depends on the zonal extent of the box because the Ekman transport error estimates increase over larger zonal integration ranges. The meridional geostrophic transport accuracy is independent of the zonal extent. [Recall that the geostrophic transport across a section with constant latitude depends only upon the difference in baroclinic streamfunction between two points, not on the distance between those points (Fofonoff 1962).]

The net zonal convergence integrated down to 50 m is accurate to within 5.3 Sv using monthly values and 1.5 Sv for the 1993–96 time mean. Degrees of freedom were estimated via an integral time scale technique (Emery and Thomson 1997). Integrated down to 200 m these error estimates increase to 17.3 Sv and 4.8 Sv. For boxes 15° of longitude wide, the net meridional convergence above 50 m is accurate to within 2.9 Sv and 0.8 Sv for monthly and time mean values; integrated down to 200 m these values increase to 6.5 Sv and 2.1 Sv, respectively. For boxes 60° of longitude wide, the net meridional convergence above 50 m is accurate to within 7.3 Sv for monthly values and 1.8 Sv for time mean values; integrated down to 200 m these values increase to 9.3 Sv and 2.6 Sv, respectively. For the full region box 100° of longitude wide, the net meridional convergence above 50 m is accurate to within 10.9 Sv (monthly) and 2.6 Sv (mean); integrated down to 200 m the estimated error is 12.3 Sv (monthly) and 3.2 Sv (mean).

The resulting accuracy for monthly values of the total vertical transport across 50 m was 6.0 Sv, 9.0 Sv, and 12.1 Sv for 15°, 60°, and 100° wide boxes, respectively. The accuracy for mean values of the total vertical transport across 50 m was 1.7 Sv, 2.3 Sv, and 3.0 Sv, respectively. For the monthly vertical transport across 200 m the accuracy was 18.5 Sv, 19.6 Sv, and 21.2 Sv for 15°, 60°, and 100° wide boxes, respectively. For the mean vertical transports across 200 m the accuracy was 5.2 Sv, 5.5 Sv, and 5.8 Sv for 15°, 60°, and 100° wide boxes, respectively. These vertical transport accuracy estimates can be converted to velocity accuracy estimates simply by dividing by the box surface areas.

The errors in the residual estimations of vertical cross-isotherm transports are a combination of the errors in the horizontal convergence and the error in the estimate of the volume of water above a particular isotherm. Meinen and McPhaden (2001) estimated the error in determining the volume of water above 20°C within 8°S–8°N, 156°E–95°W to be 1.5×10^{13} m^3 for a monthly value and 6.0×10^{12} m^3 for a roughly seven-year mean. Scaling these down for our smaller regions we estimate the accuracy of the water volume monthly (mean) values to be 1.3×10^{12} m^3 (5.2×10^{11} m^3), 5.2×10^{12} m^3 (2.1×10^{12} m^3), and 8.6×10^{12} m^3 (3.4×10^{12} m^3) for 15°, 60°, and 100° wide boxes, respectively. The corresponding rate of change errors that would impact the vertical cross-isotherm transports would be 0.7 Sv (0.3 Sv), 2.8 Sv (1.1 Sv), and 4.7 Sv (1.9 Sv) for 15°, 60°, and 100° wide boxes respectively. These estimated errors are generally quite a bit smaller than the net horizontal convergence error estimates and as such the estimated accuracy of the cross-isotherm vertical transports is nearly equivalent to the estimated accuracy of the total vertical transport at the depth of the particular isotherm.

REFERENCES

Arthur, R. S., 1960: A review of the calculation of ocean currents at the equator. *Deep-Sea Res. I,* **6,** 287–297.

Bennet, S. L., 1986: The relationship between vertical, diapycnal, and isopycnal velocity and mixing in the ocean general circulation. *J. Phys. Oceanogr.,* **16,** 167–174.

Boulanger, J.-P., and C. Menkes, 1999: Long equatorial wave reflection in the Pacific Ocean from TOPEX/POSEIDON data during the 1992–1998 period. *Climate Dyn.,* **15,** 205–226.

Brady, E. C., and H. L. Bryden, 1987: Estimating vertical velocity on the equator. *Oceanol. Acta,* Spec. Vol., 33–37.

Bryden, H. L., and E. C. Brady, 1985: Diagnostic model of the three-dimensional circulation in the upper equatorial Pacific Ocean. *J. Phys. Oceanogr.,* **15,** 1255–1273.

Busalacchi, A. J., and J. J. O'Brien, 1980: The seasonal variability in a model of the tropical Pacific. *J. Phys. Oceanogr.,* **10,** 1929–1951.

Cromwell, T., 1953: Circulation in a meridional plane in the central equatorial Pacific. *J. Mar. Res.,* **12,** 196–213.

Emery, W. J., and R. E. Thomson, 1997: *Data Analysis Methods in Physical Oceanography.* Pergamon, 634 pp.

Fine, R. A., W. H. Peterson, C. G. H. Rooth, and H. G. Östlund, 1983: Cross-equatorial tracer transport in the upper waters of the Pacific Ocean. *J. Geophys. Res.,* **88,** 763–769.

Fofonoff, N. P., 1962: Equatorial current systems. *The Sea,* Vol. 1: *Physical Oceanography,* M. N. Hill, Ed., Wiley-Interscience, 323–395.

Halpern, D., and H. P. Freitag, 1987: Vertical motion in the upper ocean of the equatorial eastern Pacific. *Oceanol. Acta,* Spec. Vol., 19–26.

——, R. A. Knox, D. S. Luther, and S. G. H. Philander, 1989: Estimates of equatorial upwelling between 140° and 110°W during 1984. *J. Geophys. Res.,* **94,** 8018–8020.

Hansen, D. V., and C. A. Paul, 1987: Vertical motion in the eastern

equatorial Pacific inferred from drifting buoys. *Oceanol. Acta,* Spec. Vol., 27–32.
Harrison, D. E., 1996: Vertical velocity in the central tropical Pacific: A circulation model perspective for JGOFS. *Deep-Sea Res. II,* **43,** 687–705.
Hayes, S. P., 1982: A comparison of geostrophic and measured velocities in the Equatorial Undercurrent. *J. Mar. Res.,* **40,** 219–229.
Jerlov, N. G., 1953: Studies of the equatorial currents in the Pacific. *Tellus,* **5,** 308–314.
Johnson, E. S., and D. S. Luther, 1994: Mean zonal momentum balance in the upper and central equatorial Pacific ocean. *J. Geophys. Res.,* **99,** 7689–7705.
Johnson, G. C., 2001: The Pacific Ocean subtropical cell surface limb. *Geophys. Res. Lett.* **28,** 1771–1774.
——, M. J. McPhaden, and E. Firing, 2001: Equatorial Pacific Ocean horizontal velocity, divergence, and upwelling. *J. Phys. Oceanogr.,* **31,** 839–849.
Joyce, T. M., R. Lukas, and E. Firing, 1988: On the hydrostatic balance and equatorial geostrophy. *Deep-Sea Res. I,* **35,** 1255–1257.
Kessler, W. S., L. M. Rothstein, and D. Chen, 1998: The annual cycle of SST in the eastern tropical Pacific, diagnosed in an ocean GCM. *J. Climate,* **11,** 777–799.
Knauss, J. A., 1963: Equatorial current systems. *The Sea.* Vol. 2: *The Composition of Sea-Water—Comparative and Descriptive Oceanography,* Wiley-Interscience, 235–252.
Lagerloef, G. S. E., G. T. Mitchum, R. B. Lukas, and P. P. Niiler, 1999: Tropical Pacific near-surface currents estimated from altimeter, wind, and drifter data. *J. Geophys. Res.,* **104,** 23 313–23 326.
Lukas, R., and E. Firing, 1984: The geostrophic balance of the Pacific Equatorial Undercurrent. *Deep-Sea Res. I,* **31,** 61–66.
McPhaden, M. J., 1981: Continuously stratified models of the steady-state equatorial ocean. *J. Phys. Oceanogr.,* **11,** 337–354.
——, 1999: Genesis and evolution of the 1997–1998 El Niño. *Science,* **283,** 950–954.
——, and X. Yu, 1999: Equatorial waves and the 1997–98 El Niño. *Geophys. Res. Lett.,* **26,** 2961–2964.
——, and Coauthors, 1998: The Tropical Ocean Global Atmosphere (TOGA) observing system: A decade of progress. *J. Geophys. Res.,* **103,** 14 169–14 240.
Meinen, C. S., and D. R. Watts, 2000: Vertical structure and transport on a transect across the North Atlantic Current near 42°N: Time series and mean. *J. Geophys. Res.,* **105,** 21 869–21 892.
——, and M. J. McPhaden, 2001: Interannual variability in warm water volume transports in the equatorial Pacific during 1993–1999. *J. Phys. Oceanogr.,* **31,** 1324–1345.
Meyers, G., 1979: Annual variation in the slope of the 14°C isotherm along the equator in the Pacific ocean. *J. Phys. Oceanogr.,* **9,** 885–891.
Philander, S. G. H., 1990: *El Niño, La Niña, and the Southern Oscillation.* Academic Press, 293 pp.
——, W. J. Hurlin, and A. D. Seigel, 1987: Simulation of the seasonal cycle of the tropical Pacific Ocean. *J. Phys. Oceanogr.,* **17,** 1986–2002.
Picaut, J., and R. Tournier, 1991: Monitoring the 1979–1985 equatorial Pacific current transports with expendable bathythermograph data. *J. Geophys. Res.,* **96,** 3263–3277.
——, S. P. Hayes, and M. J. McPhaden, 1989: Use of the geostrophic approximation to estimate time-varying zonal currents at the equator. *J. Geophys. Res.,* **94,** 3228–3236.
Pond, S., and G. L. Pickard, 1983: *Introductory Dynamical Oceanography.* 2d ed. Pergamon, 329 pp.
Poulain, P.-M., 1993: Estimates of horizontal divergence and vertical velocity in the equatorial Pacific. *J. Phys. Oceanogr.,* **23,** 601–607.
Qiao, L., and R. H. Weisberg, 1997: The zonal momentum balance of the Equatorial Undercurrent in the central Pacific. *J. Phys. Oceanogr.,* **27,** 1094–1119.
Quay, P. D., M. Stuiver, and W. S. Broecker, 1983: Upwelling rates for the equatorial Pacific Ocean derived from the bomb ^{14}C distribution. *J. Mar. Res.,* **41,** 769–792.
Ralph, E. A., and P. P. Niiler, 1999: Wind-driven currents in the Tropical Pacific. *J. Phys. Oceanogr.,* **29,** 2121–2129.
Reynolds, R. W., 1988: A real-time global sea surface temperature analysis. *J. Climate,* **1,** 75–86.
——, and T. M. Smith, 1995: A high resolution global sea surface temperature climatology. *J. Climate,* **8,** 1571–1583.
Sirven, J., C. Frankignoul, S. Février, N. Sennéchael, and F. Bonjean, 1998: Two-layer model simulations using observation and model-based wind stresses of the 1985–1992 thermocline depth anomalies in the tropical Pacific. *J. Geophys. Res.,* **103,** 21 367–21 383.
Smith, N. R., 1995a: The BMRC ocean thermal analysis system. *Aust. Meteor. Mag.,* **44,** 93–110.
——, 1995b: An improved system for tropical ocean sub-surface temperature analyses. *J. Atmos. Oceanic Technol.,* **12,** 850–870.
——, and G. Meyers, 1996: An evaluation of expendable bathythermograph and Tropical Atmosphere–Ocean Array data for monitoring tropical ocean variability. *J. Geophys. Res.,* **101,** 28 489–28 501.
Wang, W., and M. J. McPhaden, 1999: The surface-layer heat balance in the equatorial Pacific Ocean. Part I: Mean seasonal cycle. *J. Phys. Oceanogr.,* **29,** 1812–1831.
——, and ——, 2000: The surface-layer heat balance in the equatorial Pacific Ocean. Part II: Interannual variability. *J. Phys. Oceanogr.,* **30,** 2989–3009.
Weisberg, R. H., and C. Wang, 1997: Slow variability in the equatorial west central Pacific in relation to ENSO. *J. Climate,* **10,** 1998–2017.
——, and L. Qiao, 2000: Equatorial upwelling in the central Pacific estimated from moored velocity profilers. *J. Phys. Oceanogr.,* **30,** 105–124.
Wyrtki, K., 1981: An estimate of equatorial upwelling in the Pacific. *J. Phys. Oceanogr.,* **11,** 1205–1214.
——, and G. Eldin, 1982: Equatorial upwelling events in the central Pacific. *J. Phys. Oceanogr.,* **12,** 984–988.
Yu, X., and M. J. McPhaden, 1999: Seasonal variability in the equatorial Pacific. *J. Phys. Oceanogr.,* **29,** 925–947.